Nuclear Materials and Energy 000 (2016) 1–6

Contents lists available at ScienceDirect

Nuclear Materials and Energy

journal homepage: www.elsevier.com/locate/nme

Deuterium desorption from tungsten using laser heating

J.H. Yu*, M. Simmonds, M.J. Baldwin, R.P. Doerner

Center for Energy Research, University of California at San Diego, La Jolla, CA 92093-0417, USA

ARTICLE INFO

Article history:
Received 23 June 2016
Revised 30 September 2016
Accepted 14 October 2016
Available online xxx

keywords:
Tungsten
Laser
Thermal desorption
ITER divertor

ABSTRACT

Retention and desorption of hydrogenic species need to be accurately modeled to predict the tritium inventory of next generation fusion devices, which is needed both for tritium fuel recovery and for tritium safety concerns. In this paper, experiments on thermal desorption of deuterium from intrinsic polycrystalline tungsten defects using laser heating are compared to TMAP-7 modeling. The samples during deuterium plasma exposure were at a temperature of 373 K for this benchmark study with ion fluence of $0.7–1.0 \times 10^{24}$ Dm^{-2}. Following plasma exposure, a fiber laser ($\lambda = 1100$ nm) heated the samples to peak surface temperatures ranging from ~500 to 1400 K with pulse widths from 10 ms to 1 s, and 1 to 10 pulses applied to each sample. The remaining deuterium retention was measured using temperature programmed desorption (TPD). Results show that > 95% of deuterium is desorbed when the peak surface temperature reached ~950 K for > 1 s. TMAP-7 is used to predict deuterium desorption from tungsten for a range of surface temperatures and heating durations, and is compared to previous work on desorption from beryllium codeposits.

1. Introduction

The allowable inventory of tritium (T) in the plasma facing components of future tokamaks will be limited due to nuclear regulations, and thus understanding retention and release of hydrogenic species in tungsten (W) is needed for successful reactor operation. W is presently one of the leading candidates for the plasma facing wall of a fusion reactor due to its high melting temperature, high thermal conductivity, and low erosion from energetic plasma ions. There is a large body of previous work on W exposed to hydrogenic plasmas, and in particular investigating the dependence of retention on ion fluence, flux, and near steady-state surface temperature [1–3]. However, the question of how thermal desorption of hydrogenic species from W depends on both transient peak surface temperature and heating duration is not well studied. In this paper, we investigate the basic mechanisms of deuterium (D) thermal desorption using laser heating to provide a controlled temperature evolution of W samples.

Laser techniques for removal of hydrogenic species from the walls of fusion devices can be broadly categorized in terms of the laser intensity being in the ablative or non-ablative regime. High peak power densities achievable with short pulse lasers (fs to tens of ns) can easily exceed the ablation threshold for materials, and in this regime removal of hydrogenic species is accomplished by bulk erosion of material [4,5]. In contrast, lasers with intensity below the ablation threshold release trapped hydrogenic species from materials using thermal desorption, which is the regime studied here. Previous laser studies showed effective removal of hydrogen isotopes from carbon (C) codeposits when the temperature was sufficiently high (~1470 K for 1.5–3.5 ms in [6] and ~2270 K for 10 ms in [7]). However, laser heating of mixed material beryllium-carbon codeposits showed low tritium release [7], and laser heating of beryllium (Be) codeposits at lower surface temperatures (~1000 K for 10 ms) showed only ~25% D removal [8], which was in reasonable agreement with TMAP-7 modeling [9]. On W, short pulse (20 ps) laser-induced removal of D has been performed in both the ablative and non-ablative regimes, and the ablation threshold for W was found to be $\sim 1.5 \times 10^{15}$ Wm^{-2} [10]. In [11], D remained trapped in W using laser-induced desorption when the steady-state exposure temperature was > 400 K, even with relatively high laser heating up to 1800 K and with 3 ms duration.

In the present paper, we benchmark TMAP-7 modeling of hydrogenic retention and long-pulse (> 10 ms) laser-induced thermal desorption by comparing modeling results to TPD measurements. The model is then used to predict D release as a function of peak

* Corresponding author.
E-mail address: j2yu@eng.ucsd.edu (J.H. Yu).

http://dx.doi.org/10.1016/j.nme.2016.10.017

surface temperature and pulse width, with the goal of providing insight into the timescale required for hydrogenic desorption from W. Modeling may provide additional guidance for laser parameters required for laser-induced desorption spectroscopy (LIDS) on W.

2. Experimental setup

Polycrystalline W samples with grains orientated perpendicular to the surface were provided by Midwest Tungsten Service and cut into samples with 6 mm diameter and 1.5 mm thickness. All samples were ultrasonically cleaned in acetone and ethanol, and subsequently outgassed, which consisted of a linear temperature ramp of 0.5 Ks^{-1} followed by 1 h at ~1000 K.

In each D plasma exposure, four W samples were simultaneously exposed inside a plasma etcher (inductively coupled plasma source) with 1 kW of RF power at 13.56 MHz. The samples were biased to −100 V (~110 eV ion energy) and actively cooled with air to maintain a temperature of 373 K during plasma exposure, with temperature deviation being less than +/−10 K. The samples were intentionally kept cool during plasma exposure in order to obtain good signal-to-noise in the TPD signals and for accurately benchmarking TMAP-7 modeling. Plasma densities, temperatures, and D ion fluxes for the four plasma exposures used in this paper were $6–7 \times 10^{15}$ m^{-3}, 2.7–2.9 eV, and $2.0–3.4 \times 10^{20}$ $m^{-2}s^{-1}$, respectively, with total D fluence of $0.7–1.0 \times 10^{24}$ m^{-2}. The molecular ion concentrations of D^+, $D_2{}^+$, and $D_3{}^+$ were calculated to be 0.72, 0.06, and 0.22, respectively, using a model [12] based on rate balance equations and cross-section data from the literature. After plasma exposure the samples were removed from the vacuum chamber and were reloaded one-by-one, so that each sample was individually irradiated by the laser (no simultaneous plasma exposure). This procedure was repeated such that three samples were separately irradiated by the laser; the fourth sample was used as a reference and received no laser heating. The time duration between the end of plasma exposure and laser irradiation ranged from 24 to 46 hours to allow all samples to undergo the initial rapid decay of room-temperature retention, as measured in [13].

A fiber laser (Coherent Highlight 1000FL) with wavelength of 1100 nm and approximately Gaussian spatial profile was used to irradiate the W samples. Fig. 1 shows the experimental setup of the fiber laser, helicon plasma chamber, and 2-color pyrometer. Diodes optically pumped a doped fiber optic cable inside the laser. The coiled doped fiber provided a long interaction length and thus high photon conversion efficiency, producing a maximum power output of 1.07 kW with a square temporal pulse shape of variable pulse width. A water-cooled output coupler acted as the cavity mirror on one end of the doped fiber, and also transmitted laser light to a delivery fiber. Lenses were used to collimate the laser light and to provide the desired beam size at the sample. Laser light entered the plasma vacuum chamber through a laser window and traversed ~50 cm in free space to the sample, which was tilted at an angle of 20° (between the surface normal and the laser beam) so that reflected laser light would hit the water-cooled vacuum vessel wall instead of propagating backward up the optical path. Each sample was mounted and irradiated separately to ensure only one sample was heated at a time. The laser spot size ($1/e^2$ width ~ 10 mm) at the sample was larger than the sample size (6 mm diameter) to achieve a relatively uniform laser intensity across the sample. From the center of the sample to the edge, the laser intensity variation was approximately 25%, as measured with a camera imaging diffusely reflected laser light from unpolished samples. A reflectivity of 0.6 for W [14] was used in the present paper when quoting absorbed power densities.

The laser shots were monitored by a video camera and a fast 2-color pyrometer [15], both of which viewed the samples through a window in the etcher vacuum vessel. The pyrometer contained a beamsplitter and interference filters with central wavelengths of 1300 nm and 1550 nm, both with a spectral bandwidth of 100 nm. An additional filter that transmitted $\lambda > 1200$ nm was placed before the beamsplitter to minimize detection of diffusely reflected laser light from the sample. A photo-diode (PD) and a photomultiplier tube (PMT) were used to detect the 1300 and 1550 nm signals, respectively. Additional calibrated neutral density filters were used in front of the PMT as needed to avoid saturation. The temporal resolution of the PD depended on the gain and was typically < 1 ms, while the PMT had a faster response of ~10 μs. The pyrometer was calibrated using a W strip lamp with known temperature as a function of lamp current. A 2-color method was used to calculate the surface temperature, which relied on the assumption that the ratio of the sample emissivities at the two measured wavelengths during the actual measurement was the same as that during the calibration.

Following plasma exposure and laser irradiation (except for the reference samples), the samples were separately heated in the TPD oven to measure the remaining deuterium after waiting approximately one week from the time of plasma exposure. For the TPD data, the samples were heated from 300 to 1270 K at 0.5 K/s and the released D_2, HD, and H_2 were monitored by a residual gas analyzer which was calibrated with a known D_2 leak rate. During TPD, the H_2 signal was larger than the other signals by up to 4 orders of magnitude due to water vapor on the surfaces of the TPD vacuum system. This large H_2 partial pressure signal (P_{H_2}) affected the raw HD and D_2 signals (P_{HD} and P_{D_2}, respectively) due to imperfect mass filtering in the QMS, and due to the natural isotopic ratio of $D/H = 1.56 \times 10^{-4}$. Therefore a background subtraction method was used to eliminate the spurious H_2 contribution to P_{HD} and P_{D_2}, and the TPD flux of D was calculated as: $\Gamma_D = 2c(P_{D_2} - f(P_{H_2})) + c(P_{HD} - g(P_{H_2}))$, where c is the calibration factor, and f and g are background subtraction fitting functions (linear with P_{H_2}) based on the measured signals during the preheating phase and during the cool-down phase of TPD. From the use of c in the formula above, it can be seen that the sensitivity for HD is assumed to be the same as that for D_2. Compared to a simpler constant background subtraction, this more elaborate background subtraction was significant only when P_{HD}/P_{H_2} or P_{D_2}/P_{H_2} was $\lesssim 10^{-3}$.

3. TMAP-7 modeling and results

Each phase of the experiment was modeled with TMAP-7, with the three phases consisting of 1) plasma exposure, 2) laser heating, and 3) TPD. The reference sample (no laser) was used to determine the trap release energies and trap concentrations by modeling both the plasma exposure and TPD. Three traps were used with release energies of 1.02 eV, 1.27 eV, and 1.95 eV and trap concentrations of 3300 ppm, 75 ppm, and 2 ppm, respectively. Intrinsic traps were modeled and thus the distribution of traps was assumed to be uniform throughout the bulk. Trap energies were chosen based on the quality of the TMAP simulated 'fit' to the desorption maxima in TPD data. The trap concentrations were chosen to match the peak heights of the measured TPD releases, and TMAP operates on the premise of singular trap occupancy. Fig. 2 shows the TPD release D flux modeled by TMAP-7 as the black solid line, which fits reasonably well with the data shown as black circles. This reference sample had a TPD peak at 500 K and a total retention of 3.2×10^{20} Dm^{-2}, which is 4.5×10^{-4} times the plasma fluence. For 373 K plasma exposure, the TPD signal was dominated by a low energy release peak with a trap release energy at 1.02 eV. In [16], a release energy of 1.07 eV has been associated with vacancy trapping, however, low energy (0.8–1.1 eV) release energies have also been associated with impurity and dislocation trapping [17], as well as trapping at grain boundaries [13]. A trap at 1.27 eV was

Please cite this article as: J.H. Yu et al., Deuterium desorption from tungsten using laser heating, Nuclear Materials and Energy (2016), http://dx.doi.org/10.1016/j.nme.2016.10.017

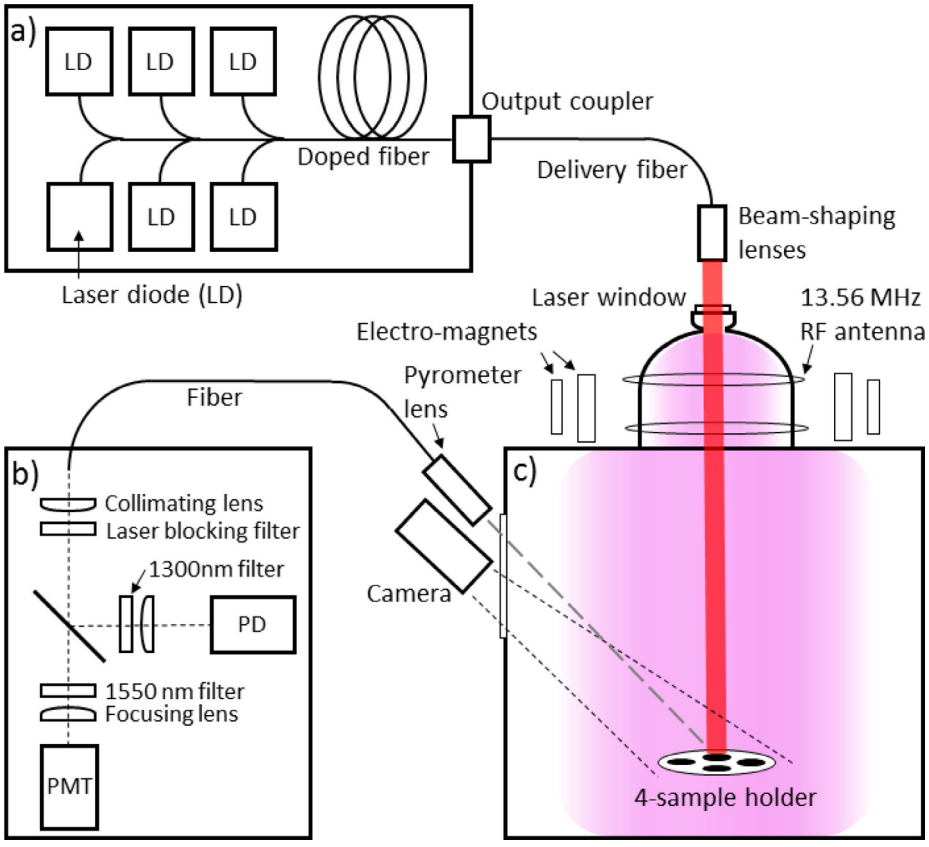

Fig. 1. Schematic of experimental setup: a) fiber laser, b) pyrometer, and c) RF plasma chamber. Laser irradiation was performed after plasma exposure.

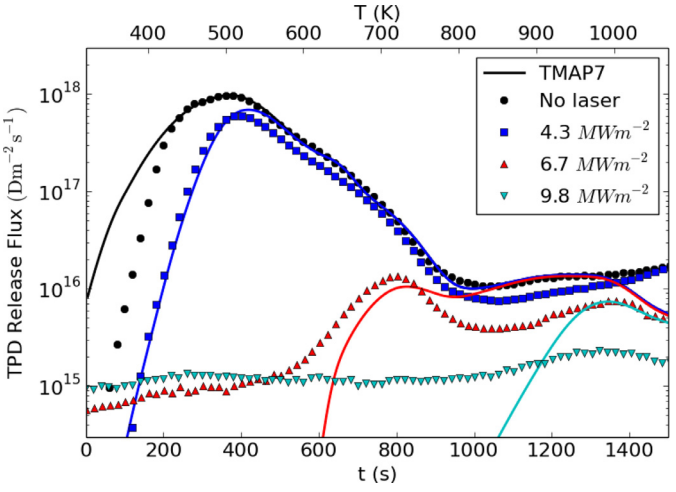

Fig. 2. Data points are TPD results from 4 samples that were simultaneously exposed to D plasma, with 3 samples subsequently laser heated before TPD. Laser pulse width was 1 s with 5 pulses on each laser-irradiated sample. The 6.7 and 9.8 MWm^{-2} cases are amplified by a factor of 5 for visibility. TMAP-7 results are shown as solid lines. .

also used in our model to achieve slightly better agreement with the data on the falling edge of the low-energy peak in the TPD temperature range of 600 to 700 K. In previous work [17], 1.1 and 1.3 eV traps were used to model TPD data from un-irradiated W and the total trap concentration from these traps was 3200 ppm, similar to the total trap concentration used in the present paper. The TPD peak in the previous work was broader than our data, and the concentrations of the 1.1 and 1.3 eV traps were 1700 ppm and 1500 ppm, respectively.

In our model the sample was implanted with D ions during plasma exposure using a 0.65 reflection coefficient and 4.5 nm implantation depth, which were based on TRIM calculations in [18]. All other parameters were taken from the Val-2d TMAP-7 model validated for tungsten [19], which uses Sievert's law for D solubility in W and Frauenfelder's diffusion coefficient [20]. The D implantation range does not support a significant temperature gradient and the Ludwig–Soret effect is not included in the model.

The model parameters for the reference sample were used to simulate D release during laser heating, as shown in Fig. 3. These samples were exposed to the same plasma as the reference sample, and subsequently each sample was irradiated separately with 5 laser pulses of various power densities. The pyrometer measurements during one laser heat pulse are shown as the data points and are used as inputs for the TMAP-7 time-dependent surface temperature when modeling desorption by the laser. Error bars on the temperature measurements were obtained by assuming a 50% uncertainty in the absolute calibration of the intensity of light detected by the pyrometer. For the 4.3 MWm^{-2} case, the aperture on the $\lambda = 1550$ nm pyrometer detector was opened to its maximum position, which allowed detection of lower T compared to the other cases. The temperature boundary condition used in TMAP-7 for the backside of the 1.5 mm thick samples was room temperature throughout the laser pulse. Note that the temperature temporal profile in the model had a short duration of 2 s between each pulse, but in the experiments the duration between each pulse was a few minutes. This does not affect the results because the amount of D desorbed from the cold sample between laser pulses was negligible.

Following the modeling of laser D desorption, TPD was modeled and the results are shown as solid lines in Fig. 2, with the 6.7 and 9.8 MWm^{-2} release fluxes multiplied by a factor of 5 for visibility. The low temperature release peak was reduced by the weaker

Please cite this article as: J.H. Yu et al., Deuterium desorption from tungsten using laser heating, Nuclear Materials and Energy (2016), http://dx.doi.org/10.1016/j.nme.2016.10.017

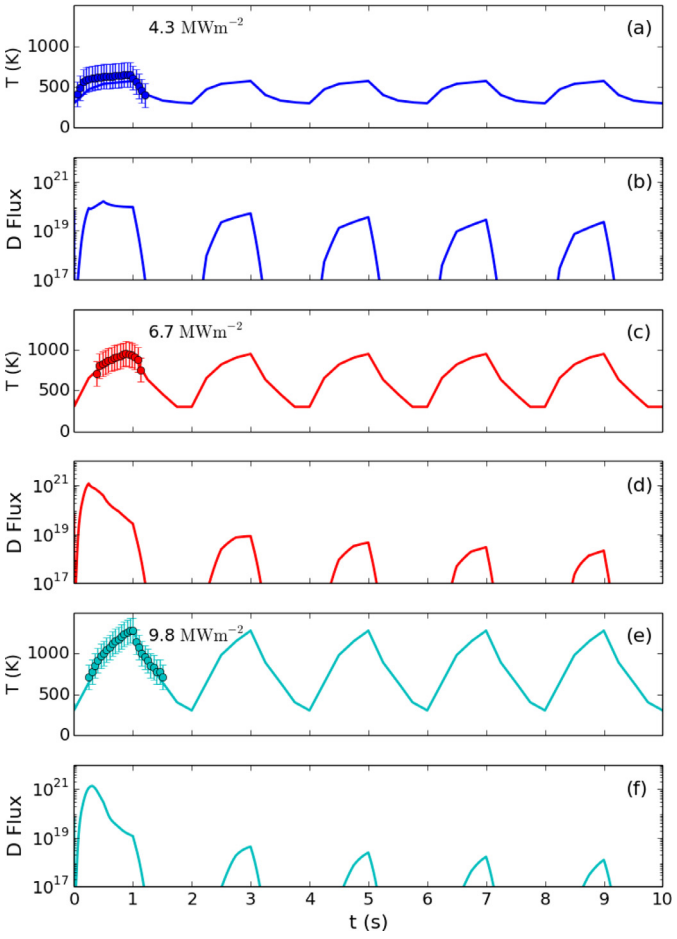

Fig. 3. Three pairs of plots are shown for three different absorbed laser power densities (color-coded with Fig. 2). In each pair, the data points in the top plot show the measured surface temperature which is used an input to TMAP-7 modeling, shown as the solid lines. The lower plots show the laser-induced desorbed D flux (units of $m^{-2}s^{-1}$) predicted by TMAP-7.

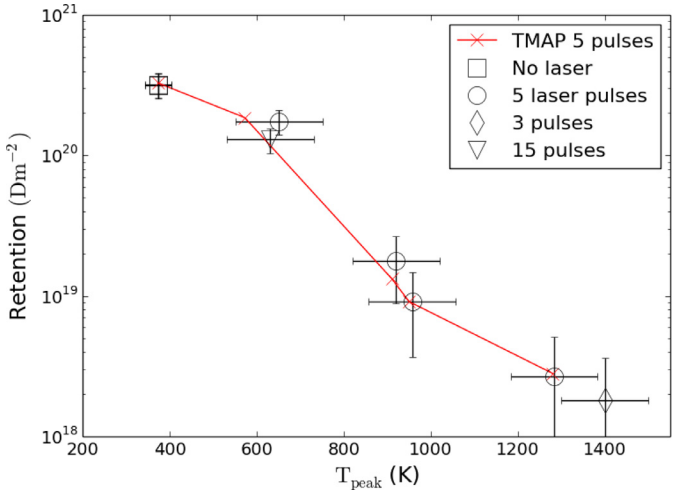

Fig. 4. The remaining D in W following laser irradiation as a function of peak surface temperature reached during the laser heat pulses. T_{peak} for the "no laser" reference case was the steady-state sample temperature during plasma exposure. The solid line shows the remaining D predicted by TMAP-7 after five 1 s heat pulses with temporal shape shown in Fig. 3, and is to be compared with the five-pulse data points shown as circles.

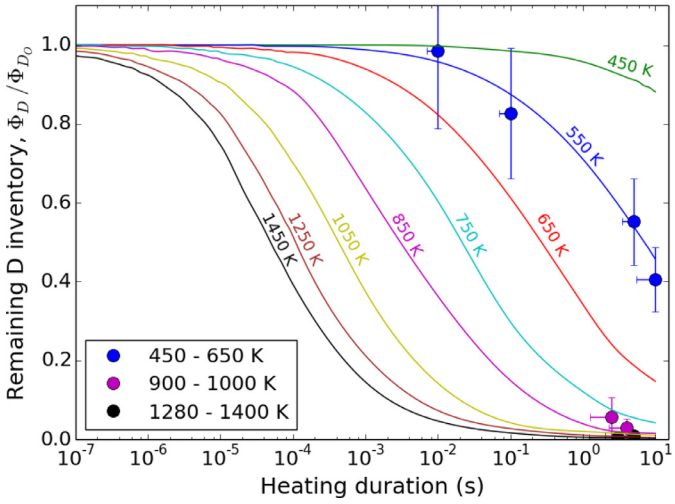

Fig. 5. Solid lines show TMAP-7 prediction of the remaining D in W as a function of heat pulse duration (square temporal shape used for the temperature evolution). Data points are the D inventory measured using TPD following laser heating, normalized to the total inventory from the reference samples.

laser pulses, while the 9.8 MWm^{-2} laser pulse with a peak temperature of 1280 K completely eliminated the low temperature TPD peak. Integrating the TPD curves gives the remaining D inventory in the samples, which is shown in Fig. 4. When the laser created a peak surface temperature of ~650 K from five 1 s heat pulses using ~4.3 MWm^{-2} of absorbed power density, ~55% of the trapped D was released from the sample.

The model was developed using the low temperature peak in the reference case, and some disagreement exists between the model and TPD data at higher release temperatures for the 6.7 and 9.8 MWm^{-2} cases. This discrepancy may be caused by the uncertainty in the TPD signals for these higher laser power cases due to the low D_2 signal (due to laser desorption) and large background H_2 signal. The high temperature (> 600 K) TPD release will be addressed in future work using a higher sample temperature during plasma exposure. In addition, NRA depth profiles of the D concentration will be used to further constrain the model.

We have extended modeling over a broad range of timescales as shown in Fig. 5, which shows the TMAP-7 prediction for laser desorption of implanted D from 373 K exposed W for a family of curves with various peak surface temperatures. The solid lines show the remaining D in W after transiently heating the sample with a square temporal temperature profile (i.e., the temperature evolution was modeled as a step function). The remaining D is normalized to the total D inventory of the reference sample, Φ_{Do}. A square temperature profile is used here for simplicity because the exact temperature evolution depends on the temporal shape of the heat pulse [15] and the boundary conditions on the backside of the sample. The data points are plotted at time durations on the x-axis equal to $N\tau$, where N is the number of pulses and τ is the laser pulse width. However, the actual surface temperature temporal profiles have a finite rise time. Thus, half-error bars are plotted with their lengths determined from the time Δt that the measured T_{surf} (with error bars) lies within the temperature ranges shown in the legend of Fig. 5, with the half-error bar lengths given by $N\Delta t$.

The amount of D released from thermal LID depends not only on the peak surface temperature, but also on the duration of laser heating. This is because trapped D has a higher probability of escaping with longer heating times, and also because a longer heat pulse penetrates deeper within the bulk.

Please cite this article as: J.H. Yu et al., Deuterium desorption from tungsten using laser heating, Nuclear Materials and Energy (2016), http://dx.doi.org/10.1016/j.nme.2016.10.017

4. Discussion

The majority of tritium inventory in ITER will be in Be/T codeposits. Previous work on laser-induced thermal desorption from ~1 μm thick Be/D codeposits showed that only ~25% of the trapped D was released at peak surface temperatures of ~1000 K with a heat pulse duration of 10 ms [8]. Modeling showed reasonable agreement with these earlier experiments, and predicted that the release of D from Be/D codeposits strongly depends on the Be/D layer thickness [9]. This was also shown by simulations in [21], which further showed the dependence of D release on heating duration. That modeling predicted ~92% of the trapped inventory was released from a 10 μm Be/D deposit after 10 s of heating with surface temperature of 1100 K, but only ~50% was released after 1 s.

The D desorption characteristics of Be/D codeposits is in contrast to the present work on W, in which nearly all D is removed from 373 K exposed W when the peak surface temperature is > 1000 K for a heating duration > 1 s. Using a shorter heat duration of 10 ms, our modeling of W predicts that ~80% of D is released with $T_{surf} = 1000$ K, as seen from Fig. 5. The fraction of D released is expected to depend on the steady-state exposure temperature of W during D implantation, and this will be the subject of future work.

The higher rate of D release from W compared to Be/D codeposits is due to differences in trap concentrations, material characteristics, and possibly due to differences in the depth distribution of D. In the Be/D models [9,21], the trap concentrations were 10–100x higher than that for W. Thus, the multi-step process of de-trapping, migration, and re-trapping in the codeposit appears to limit D release. In addition, the surface recombination of D on W is known to be much faster than that on Be (e.g., compare [22] and [23]). Finally, the distribution of D is uniform throughout a Be/D layer, while D diffusing into 373 K W during implantation reaches a maximum depth of a few μm [24].

5. Conclusion

This work is a benchmark study of long-pulse (> 10 ms) laser-based thermal desorption of D from intrinsic traps in 373 K exposed polycrystalline W. TMAP-7 modeling of plasma exposure, laser heating, and TPD, captures the basic features of the processes using 3 traps with release energies of 1.02 eV, 1.27 eV, and 1.95 eV. The model and the data show that D release depends on both surface temperature and heating duration, with laser heating desorbing nearly all (> 99%) trapped D when the surface temperature reaches 1280 K for 1 s pulse widths. At the other extreme of our data range, laser heating for 10 ms up to ~500 K shows that <~ 5% is released. The release characteristics of W are compared to previous work on Be/D codeposits, and the larger release rate of D from W compared to that from Be/D is attributed to differences in material properties (such as the higher surface recombination rate of D on W) and to the higher trap concentration in codeposits (due to the presence of BeD).

Future work includes performing laser thermal desorption on W samples with ITER-relevant temperatures during plasma exposure. At higher steady-state surface temperatures and plasma exposure duration, D diffuses deeper in the W bulk and could also be trapped in defects with higher release energy. While a higher W temperature will decrease the amount of trapped D in undamaged W, the hydrogenic inventory in the ITER W divertor will not be negligible because fusion neutrons will create additional defects that act as trap sites in W [25–27]. Thus, future work also includes studying laser desorption at elevated temperatures in displacement-damaged W.

Acknowledgment

This work was supported by US DOE grant DE-FG02-07ER54912.

References

[1] Y.Z. Jia, G. De Temmerman, G.N. Luo, H.Y. Xu, C. Li, B.Q. Fu, W. Liu, Surface morphology and deuterium retention in tungsten exposed to high flux D plasma at high temperatures, J. Nucl. Mater. 457 (2015) 213–219, doi:10.1016/j.jnucmat.2014.11.079.
[2] M.H.J. 'T Hoen, B. Tyburska-Püschel, K. Ertl, M. Mayer, J. Rapp, A.W. Kleyn, P.A. Zeijlmans van Emmichoven, Saturation of deuterium retention in self-damaged tungsten exposed to high-flux plasmas, Nucl. Fusion. 52 (2012) 023008, doi:10.1088/0029-5515/52/2/023008.
[3] O.V. Ogorodnikova, J. Roth, M. Mayer, Deuterium retention in tungsten in dependence of the surface conditions, J. Nucl. Mater. 313-316 (2003) 469–477, doi:10.1016/S0022-3115(02)01375-2.
[4] C. Grisolia, A. Semerok, J.M. Weulersse, F. Le Guern, S. Fomichev, F. Brygo, P. Fichet, P.Y. Thro, P. Coad, N. Bekris, M. Stamp, S. Rosanvallon, G. Piazza, In-situ tokamak laser applications for detritiation and co-deposited layers studies, J. Nucl. Mater. 363–365 (2007) 1138–1147, doi:10.1016/j.jnucmat.2007.01.169.
[5] C. Hernandez, H. Roche, C. Pocheau, C. Grisolia, L. Gargiulo, A. Semerok, A. Vatry, P. Delaporte, L. Mercadier, Development of a Laser Ablation System Kit (LASK) for Tokamak in vessel tritium and dust inventory control, Fusion Eng. Des. 84 (2009) 939–942, doi:10.1016/j.fusengdes.2008.12.033.
[6] B. Schweer, F. Irrek, G. Sergienko, V. Philipps, U. Samm, In situ diagnostic for monitoring of deuterium and tritium in re-deposited carbon layers by laser induced desorption, J. Nucl. Mater. 363–365 (2007) 1375–1379, doi:10.1016/j.jnucmat.2007.01.247.
[7] C.H. Skinner, N. Bekris, J.P. Coad, C.A. Gentile, M. Glugla, Tritium removal from JET and TFTR tiles by a scanning laser, J. Nucl. Mater. 313–316 (2003) 496–500, doi:10.1016/S0022-3115(02)01382-X.
[8] J.H. Yu, M.J. Baldwin, R.P. Doerner, R.A. Pitts, R.D. Smirnov, H.W. Xu, Desorption of deuterium from beryllium codeposits using flash heating, J. Nucl. Mater. 438 (2013) 1150–1154, doi:10.1016/j.jnucmat.2013.01.254.
[9] M.J. Baldwin, T. Schwarz-Selinger, J.H. Yu, R.P. Doerner, TMAP-7 simulation of D2 thermal release data from Be co-deposited layers, J. Nucl. Mater. 438 (2013) S967–S970, doi:10.1016/j.jnucmat.2013.01.210.
[10] K. Hirata, K. Furumoto, N. Yamamoto, T. Tanabe, Application of pulsed laser irradiation for removal of hydrogen retained in tungsten, J. Nucl. Mater. 443 (2013) 298–301, doi:10.1016/j.jnucmat.2013.07.047.
[11] M. Zlobinski, V. Philipps, B. Schweer, A. Huber, M. Reinhart, S. Möller, G. Sergienko, U. Samm, M.H.J. Hoen, A. Manhard, K. Schmid, Hydrogen retention in tungsten materials studied by laser induced desorption, J. Nucl. Mater. 438 (2013) S1155–S1159, doi:10.1016/j.jnucmat.2013.01.255.
[12] E.M. Hollmann, A.Y. Pigarov, Measurement and modeling of molecular ion concentrations in a hydrogen reflex-arc discharge, Phys. Plasmas. 9 (2002) 4330–4339, doi:10.1063/1.1503070.
[13] R. Bisson, S. Markelj, O. Mourey, F. Ghiorghiu, K. Achkasov, J.M. Layet, P. Roubin, G. Cartry, C. Grisolia, T. Angot, Dynamic fuel retention in tokamak wall materials: an in situ laboratory study of deuterium release from polycrystalline tungsten at room temperature, J. Nucl. Mater. 467 (2015) 432–438, doi:10.1016/j.jnucmat.2015.07.028.
[14] G.G. van Eden, T.W. Morgan, H.J. van der Meiden, J. Matejicek, T. Chraska, M. Wirtz, G. De Temmerman, The effect of high-flux H plasma exposure with simultaneous transient heat loads on tungsten surface damage and power handling, Nucl. Fusion 54 (2014) 123010, doi:10.1088/0029-5515/54/12/123010.
[15] J.H. Yu, G. De Temmerman, R.P. Doerner, R.A. Pitts, The effect of transient temporal pulse shape on surface temperature and tungsten damage, Nucl. Fusion (2015) 55, doi:10.1088/0029-5515/55/9/093027.
[16] M. Poon, A.A. Haasz, J.W. Davis, Modelling deuterium release during thermal desorption of D+-irradiated tungsten, J. Nucl. Mater. 374 (2008) 390–402, doi:10.1016/j.jnucmat.2007.09.028.
[17] M. Shimada, G. Cao, Y. Hatano, T. Oda, Y. Oya, M. Hara, P. Calderoni, The deuterium depth profile in neutron-irradiated tungsten exposed to plasma, Phys. Scr. T145 (2011) 014051, doi:10.1088/0031-8949/2011/T145/014051.
[18] J.P. Biersack, W. Eckstein, Sputtering studies with the Monte Carlo Program TRIM.SP, Appl. Phys. A Solids Surfaces. 34 (1984) 73–94, doi:10.1007/BF00614759.
[19] J. Ambrosek, G.R. Longhurst, Verification and Validation of TMAP7, 2008.
[20] R. Frauenfelder, Solution and diffusion of hydrogen in tungsten, J. Vac. Sci. Technol. 6 (1969) 388, doi:10.1116/1.1492699.
[21] E.E. Mukhin, P. Andrew, A.D. Anthoine, A.N. Bazhenov, R. Barnsley, I.M. Bukreev, V.L. Bukhovets, A.P. Chernakov, A.E. Gorodetsky, M.M. Kochergin, A.N. Koval, A.B. Kukushkin, A.S. Kukushkin, G.S. Kurskiev, M.G. Levashova, A.E. Litvinov, V.N. Litunovsky, A.V. Markin, I.V. Mazul, S.V. Masyukevich, I.V. Miroshnikov, A.S. Nemov, A.N. Novokhatsky, A.G. Razdobarin, E.V. Sherstnev, D.S. Samsonov, V.V. Semenov, A.S. Smirnov, G. De Temmerman, S.Y. Tolstyakov, R.K. Zalavutdinov, M.J. Walsh, *In situ* monitoring hydrogen isotope retention in ITER first wall, Nucl. Fusion. 56 (2016) 036017, doi:10.1088/0029-5515/56/3/036017.
[22] R.A. Causey, T.J. Venhaus, The use of tungsten in fusion reactors: a review of the hydrogen retention and migration properties, Phys. Scr. T94 (2001) 9–15.
[23] R.A. Causey, K.L. Wilson, Tritium inventory and permeation in the ITER beryllium, J. Nucl. Mater. 212-215 (1994) 1436–1442.

Please cite this article as: J.H. Yu et al., Deuterium desorption from tungsten using laser heating, Nuclear Materials and Energy (2016), http://dx.doi.org/10.1016/j.nme.2016.10.017

[24] J.L. Barton, Y.Q. Wang, R.P. Doerner, G.R. Tynan, Development of an analytical diffusion model for modeling hydrogen isotope exchange, J. Nucl. Mater. 463 (2015) 1129–1133, doi:10.1016/j.jnucmat.2014.12.116.
[25] M. Shimada, G. Cao, T. Otsuka, M. Hara, M. Kobayashi, Y. Oya, Y. Hatano, Irradiation effect on deuterium behaviour in low-dose HFIR neutron-irradiated tungsten, Nucl. Fusion. 55 (2015) 013008, doi:10.1088/0029-5515/55/1/013008.
[26] Y. Hatano, M. Shimada, T. Otsuka, Y. Oya, V.K. Alimov, M. Hara, J. Shi, M. Kobayashi, T. Oda, G. Cao, K. Okuno, T. Tanaka, K. Sugiyama, J. Roth, B. Tyburska-Püschel, J. Dorner, N. Yoshida, N. Futagami, H. Watanabe, M. Hatakeyama, H. Kurishita, M. Sokolov, Y. Katoh, Deuterium trapping at defects created with neutron and ion irradiations in tungsten, Nucl. Fusion. 53 (2013) 073006, doi:10.1088/0029-5515/53/7/073006.
[27] O.V. Ogorodnikova, K. Sugiyama, Effect of radiation-induced damage on deuterium retention in tungsten, tungsten coatings and Eurofer, J. Nucl. Mater. 442 (2013) 518–527, doi:10.1016/j.jnucmat.2013.07.024.

Please cite this article as: J.H. Yu et al., Deuterium desorption from tungsten using laser heating, Nuclear Materials and Energy (2016), http://dx.doi.org/10.1016/j.nme.2016.10.017